Carbon 184 (2021) 941–948

Contents lists available at ScienceDirect

Carbon

journal homepage: www.elsevier.com/locate/carbon

Research Paper

Direct measurement of carbon nanotube temperature between fiber ferrules as a universal tool for saturable absorber stability investigation

Diana Galiakhmetova [a, b], Yuriy Gladush [a, *], Aram Mkrtchyan [a], Fedor S. Fedorov [a], Eldar M. Khabushev [a], Dmitry V. Krasnikov [a], Raghavan Chinnambedu-Murugesan [b], Egor Manuylovich [b], Vladislav Dvoyrin [b, c], Alex Rozhin [b], Mark Rümmeli [d, e, f, g], Sergey Alyatkin [a], Pavlos Lagoudakis [a], Albert G. Nasibulin [a, h, **]

[a] Skolkovo Institute of Science and Technology, Moscow, 121205, Russia
[b] Aston Institute of Photonic Technologies, Aston University, Birmingham, B4 7ET, United Kingdom
[c] Novosibirsk State University, Novosibirsk, 630090, Russia
[d] Soochow Institute for Energy and Materials Innovations, College of Energy, Collaborative Innovation Center of Suzhou Nano Science and Technology, Key Laboratory of Advanced Carbon Materials and Wearable Energy Technologies of Jiangsu Province, Soochow University, Suzhou, 215006, China
[e] Centre of Polymer and Carbon Materials, Zabrze, 41-819, Poland
[f] Center for Energy and Environmental Technologies, Ostrava, 708 33, Czech Republic
[g] Leibniz Institute for Solid State and Materials Research Dresden, Dresden, 01069, Germany
[h] Aalto University, Espoo, P.O. Box 151100, FI-00076, Finland

ARTICLE INFO

Article history:
Received 20 April 2021
Received in revised form
8 August 2021
Accepted 13 August 2021
Available online 16 August 2021

Keywords:
Carbon nanotubes
Thermal stability
Saturable absorption
Ultra-fast lasers

ABSTRACT

Single-walled carbon nanotubes (SWCNTs) are widely explored for the ultrashort pulse generation in the fiber lasers enabled by pronounced saturable absorption (SA) effect. Despite many remarkable results demonstrated in the area, degradation of the samples inside the laser cavity limits the widespread use of SWCNT-SA. In the present work, we investigate the degradation mechanism by measuring the temperature of the carbon nanotubes in an operating laser cavity in accordance with the Raman G-band position. We identify the process behind the sample degradation by comparing the burning temperature of the sample with results of thermogravimetric analysis. We apply this approach for the SWCNTs in polyvinyl alcohol polymer matrix and polymer-free SWCNT thin film and demonstrate that these samples undergo different degradation mechanism. Proposed technique provides a useful instrument for optimization of SWCNT-SA for desired ultrafast laser generation.

1. Introduction

Single-walled carbon nanotubes (SWCNTs) are known to demonstrate high optical nonlinearity promising various applications in optoelectronics and photonics [1]. Among them the implementation of carbon nanotubes as a saturable absorber (SA) for ultrafast pulse generation in the fiber lasers is the most promising and well established [2–4]. Low saturation power, ultra-fast optical response around 1 ps and high environmental stability of SWCNT-SA allowed to demonstrate excellent pulse properties: pulse width below 100 fs [5], high energy pulse generation [6] and broadband operation across 1–2 μm spectral range [7]. Moreover, excellent physical properties of SWCNT-SA are accompanied with the relative simplicity of fabrication (compared to conventional semiconductor saturable absorber mirrors, SESAMs) and a variety of implementation techniques. The easiest and the most widely used technique comprises clamping carbon nanotubes between two connectors either dispersed in polymer matrix, i.e. as a polymer composite [8–10] or as a polymer-free SWCNT film deposited by spray deposition [11], thermo-diffusion [12] or dry transfer technique [13].

Unfortunately, incessant irradiation may lead to degradation of

* Corresponding author.
** Corresponding author. Skolkovo Institute of Science and Technology, Moscow, 121205, Russia.
E-mail addresses: diana.galiakhmetova@skoltech.ru (D. Galiakhmetova), y.gladush@skoltech.ru (Y. Gladush), a.nasibulin@skoltech.ru (A.G. Nasibulin).

https://doi.org/10.1016/j.carbon.2021.08.032
0008-6223/

the sample when incident laser power exceeds a certain limit. Usually, the threshold average power of several tens of milliwatts inside the fiber cavity is reported, under which SWCNT-SA burns down with a subsequent loss of mode-locking. The interaction of absorbing material with ultra-short pulses may give rise to various phenomena like optical breakdown, multi-photon absorption and ionization leading to chemical bonds breaking, and, finally, non-thermal phase-transitions or ablation [14,15]. The single pulse ablation of carbon nanotubes was investigated in several works, where critical fluence depending on the SWCNT sample preparation technique, laser wavelength and pulse width were reported to vary from 25 to 500 mJ/cm^2 [16–18]. On the other hand, the small heat capacity of the carbon nanotubes may lead to fast heating and subsequent thermal degradation of the sample. In this case, the degradation process will be governed by the average power of the radiation rather than by laser pulse fluence. The contribution of each mechanism can be strongly dependent on the sample preparation technique. For polymer/SWCNT composites, the degradation temperature of an organic polymers is usually around 120–200 °C, which is 2–3 times smaller than that for pristine carbon nanotubes reaching 400–500 °C under ambient conditions [19]. Though a polymer matrix itself is chosen to be transparent at laser frequency, it can be heated by carbon nanotubes, leading to irreversible damage of the SWCNT-SA [20]. Chernysheva et al. reported a crater formation within a polyvinyl alcohol (PVA)/SWCNT composite that leads to decreased transmittance and modulation depth [21]. In contrast, Ryu et al. reported increased transmittance under continuous light illumination if power exceeds 5 mW for PVA/SWCNT film sandwich-like structure [22]. Yoon et al. examined carbon nanotubes directly deposited on fiber ferrule by spay and optical deposition methods [23]. The authors demonstrated combustion of the film at an average power ranging from 20 to 40 mW for standard 9 μm core fibers. These works clearly demonstrate non-similar degradation behaviors and provide information on stability aspects of the SWCNT-SA, but do not shine light on degradation mechanism. Thermal stability can be significantly increased by introducing the evanescent field interaction when SWCNTs are deposited on a side-polished fiber [24–26], a tapered fiber [27,28] or inside a hollow core fiber [29]. Though the method increases the damage threshold, other drawbacks emerge. It has typically higher saturation power, D-shape fibers have polarization-dependent absorption, tapered fibers are highly fragile, and hollow-core fiber is difficult to integrate inside the all-fiber scheme. Moreover, all these methods are much more complicated in fabrication. Development of robust and stable SWCNT-SA for on-ferrule implementation remains an actual problem that requires a better understanding of the degradation mechanisms involved.

One of the ways to distinguish between degradation mechanisms associated with ultra-short pulse action and heating induced burning, is to measure the temperature of the samples in the laser cavity. Though SWCNT-SA is clamped between two connectors and cannot be observed directly, one can access the temperature by measuring SWCNT Raman G and 2D band positions, which shows linear temperature dependence [30,31].

In the present work, we investigate the mechanism of the carbon nanotube saturable absorber degradation by measuring the temperature of SWCNT-SA clamped between two connectors in the conditions identical to the laser cavity. We illuminate a sample with a laser radiation from ultra-fast erbium fiber laser and additionally couple a small power green laser through the wavelength division multiplexer (WDM) to measure the Raman spectra of the carbon nanotubes and to assess the temperature of the saturable absorber as a function of intracavity power. We compare three types of samples and show that different degradation mechanisms dominate for pure SWCNTs and composite samples.

2. Sample preparation and characterization

In our study, we compare three types of samples, two of them are PVA/SWCNT polymer composites, and the third one is a polymer-free thin film of carbon nanotubes. For the composite samples, we used commercially available HiPco carbon nanotubes and SWCNTs synthesized by laser ablation method [32]. An average diameter of HiPco and laser ablation SWCNTs is 1.2 nm and 1.3 nm, respectively. The sample preparation is described in detail in Materials and Methods. In brief, carbon nanotubes powder was dispersed in water with sodium dodecylbenzenesulfonate (SDBS) surfactant. After sonication and ultracentrifugation, the supernatant solution was mixed with dissolved polyvinyl alcohol that forms a film after the water evaporation. Obtained samples were cut (~1 × 1 mm^2) and sandwiched between two standard fiber ferrules with an index-matching gel.

Polymer-free SWCNTs were synthesized by an aerosol CVD method. SWCNTs grow in the hot reactor zone on catalyst nanoparticles floating in CO atmosphere [33]. At the outlet of a quartz tubular reactor, aerosol of SWCNTs was collected on a nitrocellulose filter followed by dry-transfer on a connector [34] (more in Materials and Methods). It should be mentioned that the methods for the synthesis and transfer do not involve any liquid chemistry steps and ensure the absence of any organic compounds in the samples of aerosol synthesized SWCNTs.

In the following, the samples described above will be referred to as PVA/HiPco, PVA/Ablation and Aerosol SWCNTs.

All the samples are chosen so that S_{11} transition covers the laser line at 1550 nm. PVA/HiPco and aerosol CVD samples have nearly the same transmittance at 1550 nm of 79% and 74%, respectively, while PVA/Ablation is much darker with a 12% transmittance (Fig. 1a). The high quality of the carbon nanotubes is ensured by the Raman spectra shown in Fig. 1b. The ratio of intensities of G and D bands (I_G/I_D) is 19, 21 and 60 for HiPco, laser ablation and aerosol SWCNTs, respectively. Pronounced shoulders to the left of G-band evidence for the presence of metallic nanotubes in the mixtures. When measuring the dependence of the G-band position as a function of temperature in a heating cell, we observed no significant line deformation under heating for all the samples (Fig. S1). The G band shift coefficients are -0.029 ± 0.004 cm^{-1}K^{-1}, -0.025 ± 0.005 cm^{-1}K^{-1} and -0.019 ± 0.004 cm^{-1}K^{-1} for HiPco, laser ablation and aerosol CVD SWCNTs, respectively (Fig. S2), obtained from averaging over different points across the film. These numbers are in agreement with corresponding values measured by other groups [31,35].

3. Results and discussion

3.1. Laser operation

Prior to the stability studies, we compare the performance of the samples inside the laser cavity. We use an erbium-doped fiber laser in the ring cavity configuration with a total length of 5 m and net dispersion of −0.085 ps^2 (see Materials and methods for more details). All three samples demonstrate a stable single-pulse mode-locking regime with sub-picosecond pulse width with relatively close parameters (Fig. 2). Single pulse generation is reached at different pump power for each sample, so the regimes are compared at the maximum pump power of a stable single pulse operation window. PVA/HiPco needs the lowest pump power for mode locked operation self-starting corresponding to 36.6 mW. At 44.8 mW of pump power, the single pulse operation regime is sustained with pulse duration of 825 fs, 3.2 nm spectral width, 7 mW output power and 0.17 nJ pulse energy. PVA/Ablation composite self-starts at 38 mW of pump power. At 40 mW of pump

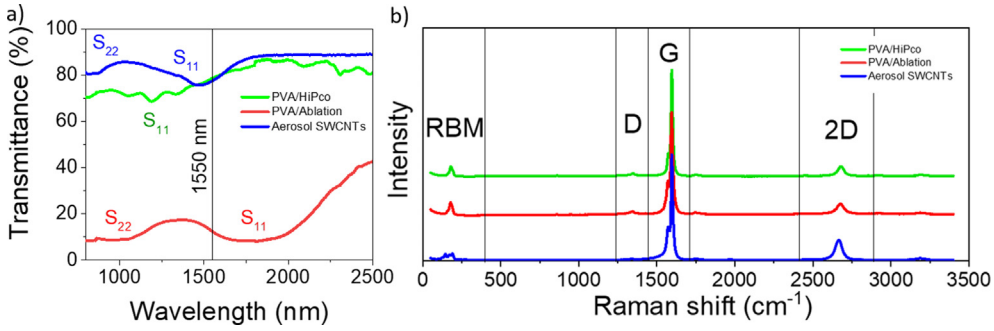

Fig. 1. SWCNTs optical properties. (a) Transmittance spectra of the SWCNT samples. Black line indicates the position of the laser working wavelength. (b) Raman spectra clearly demonstrate high G/D ratio for all the SWCNT samples under consideration. (A colour version of this figure can be viewed online.)

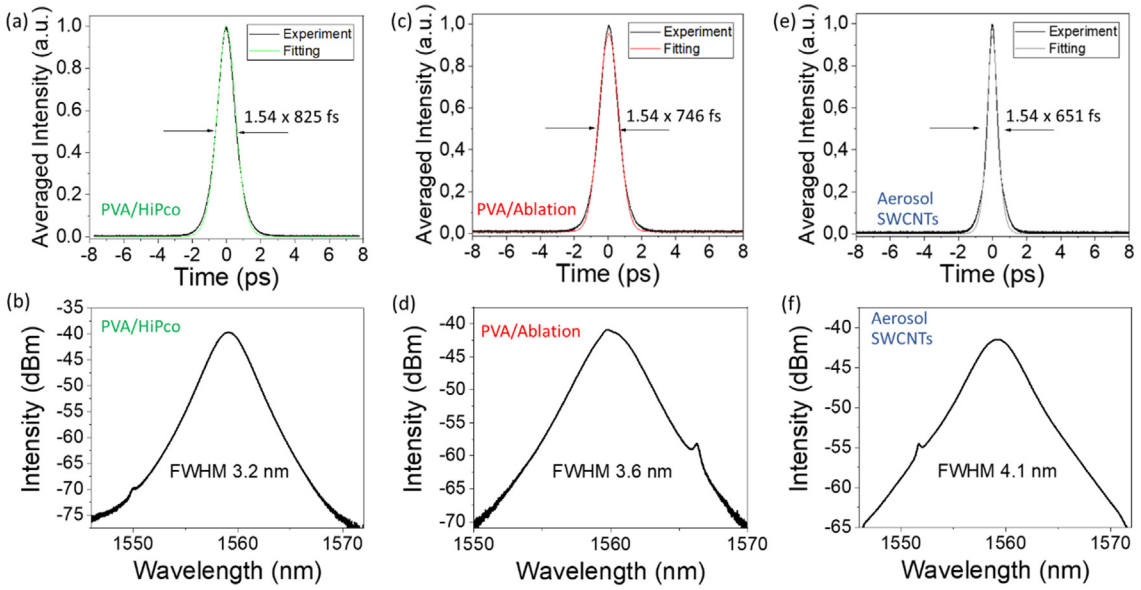

Fig. 2. Laser pulse properties for mode-locked regimes obtained with a saturable absorbers based on (a–b) PVA/HiPco, (c–d) PVA/Ablation, and (e–f) aerosol SWCNTs. The top panel is experimental pulse autocorrelation function and its *sech*^{2} fit. The bottom panel is pulse spectra. (A colour version of this figure can be viewed online.)

power, it shows pulse duration of 746 fs, 3.4 nm spectral width, 6.2 mW output power and 0.15 nJ pulses. Aerosol SWCNTs demonstrate the highest self-starting pump power at 55.4 mW. At the same time, they show the shortest pulse duration of 650 fs and 3.9 nm spectral width, output power of 9.5 mW and 0.23 nJ pulses. Slightly shorter pulse duration can be attributed to larger modulation depth of the sample (see Fig. S5). Overall, for all the saturable absorbers under consideration we observe a very small difference in the pulse parameters, which is mostly defined by the fiber laser parameters, namely, dispersion and nonlinearity, in agreement with other numerical and experimental findings [36–38].

3.2. Thermogravimetric analysis

Thermal decomposition of PVA composites was investigated in a number of works [39–42], where decomposition temperatures in a range from 180 to 320 °C are reported depending on the composite filling and preparation technique. To evaluate the decomposition temperatures of our samples, we performed simultaneous thermal analysis, i.e. thermogravimetric analysis (TGA), differential scanning calorimetry (DSC) coupled with mass spectrometry (MS) for all three types of samples. The TGA results are shown in Fig. 3.

Both PVA-based composites show a similar behavior. Further,

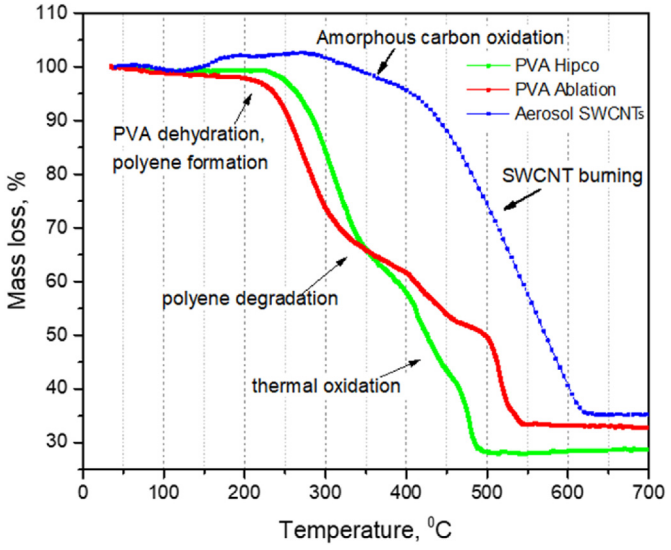

Fig. 3. Termogravimetric analysis. Mass loss under heating for PVA/HiPco (green), PVA/Ablation (red) and Aerosol SWCNTs (blue); the main processes are noted in the graph. (A colour version of this figure can be viewed online.)

we discuss PVA/Ablation sample as a representative example. At 60 °C, we observe minor mass loss due to the liberation of physisorbed water. When the temperature reaches 200 °C a drastic change in mass is detectable stemming from partial dehydration of the PVA with removal of −OH hydroxyl groups that yields polyene formation with mass loss of *ca.* 36% [39]. At this point irreversible decomposition takes place. This process is followed by polyene degradation at *ca.* 400 °C giving macroradicals whose destruction and decomposition leads to appearance of various compounds like acetaldehyde, benzaldehyde [40], ethanol [39,41] and other products [43]. A polyene cross-linking in the oxidative environment should be also anticipated [40]. The next stage starts from 490 °C and might be assigned to thermal oxidation of carbonized residue, which is formed at previous stages. At about 530 °C, we notice a change in mass which could probably be related to continuous CNT oxidation. Total weight loss when heated up to 800 °C is *ca.* 67.5%. Comparing the TGA results of two composites, we identify the temperature shift of the mass loss curve around of 230 °C. This difference can be described by the difference in CNT concentration and type resulting in dissimilar thermal conductivity. More details, DSC and MS results can be found in Supplementary materials.

Aerosol SWCNTs are characterized by stepwise changes in mass related to processes water desorption, followed by oxidation of iron catalyst nanoparticles, left after the synthesis, what is manifested by mass increase and then by oxidation of amorphous carbon starting around 280 °C. We do not observe any influence of these processes on nonlinear optical response at 1550 nm. SWCNT oxidation starts at 440 °C which defines the critical temperature for this sample (Fig. 3) [44]. These results are in agreement with other studies that reported carbon nanotubes degradation around 500 °C [19,45,46].

3.3. SWCNT temperature measurements

Now we discuss the temperature measurement of the SWCNT-SA clamped between two connectors on the output of the working laser by simultaneous measurement of the Raman shift. For this, we modify the laser scheme and build the setup for the Raman spectrum measurement as shown in Fig. 4. We insert two identical SWCNT samples clamped between two connectors – one in the resonator is used to produce ultra-short pulse generation, and the other one is a test sample located on the output fiber of the laser.

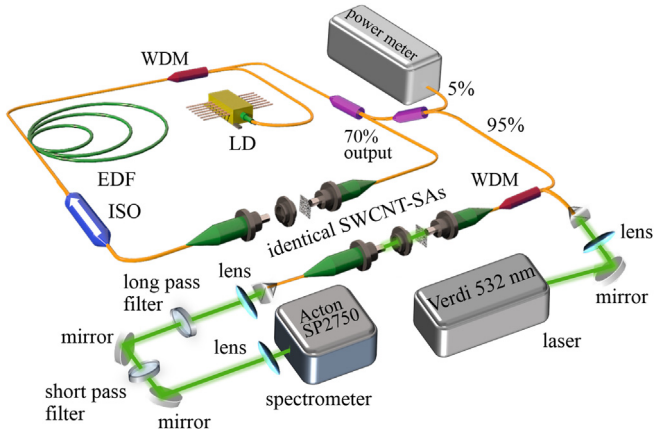

Fig. 4. Laser scheme and measuring setup. Laser scheme comprise of a standard ring cavity with SWCNT-SA on the fiber ferrules, an isolator (ISO), erbium doped fiber (EDF), a wave division multiplexer (WDM) and a splitter returning 30% back to the cavity. On the output, we use 5% for laser power monitoring. Green laser is coupled into the fiber through the WDM and pass through identical SWCNT-SA and then all the light is coupled to the spectrometer. (A colour version of this figure can be viewed online.)

The test sample is additionally illuminated with the green laser inserted through the WDM prior to which we insert 95/5 coupler to monitor incident fiber laser power. The power of the green laser is set to 0.5 mW so that the heating by this laser is below 10° for each of the samples. Laser output coupler is 70/30 where 70% goes to output, and 30% goes to resonator so that the fiber laser power is the same on both samples and we can expect identical heating temperatures. On the output, we couple the Raman signal to the spectrometer and measure the shift of the G-band depending on the incident power.

For each sample, we performed a series of Raman measurement cycles increasing maximum incident power until the mode-lock generation breaks down due to the sample damage. The Raman shift is shown in Fig. 5(a–c) for PVA/HiPco, PVA/Ablation and Aerosol SWCNTs, correspondently. The fire icon represents the point where SWCNT-SA burns with breaking of mode locking. It is accompanied by the disappearance of SWCNT Raman features on the test sample at nearly the same power. A discrepancy in damage power for SA and test sample may come from the small difference in their properties, i.e. thickness variation, an uncontrollable gap between ferrule and the sample, etc. At low power all the samples show nearly linear G-band shift as function of incident power. We attribute it to the heating of the samples, the corresponding temperatures are plotted in Fig. 5(d–e). The shaded region on the plots represents the uncertainty in the temperature determination defined by dispersion of Raman band shift coefficient. As expected, the darkest PVA/Ablation sample reaches higher temperatures at much smaller average power compared to PVA/HiPco. For both PVA-based composites, curves for the first cycle and for the second one do not coincide. Samples heat up faster in the second cycle, which we attribute to increased absorption of the sample. Under average power of around 25 mW for PVA/HiPco, the heating accelerates, and then, at 33 mW, it changes the sign of the G-band shift to the opposite. The same behavior we observe for the PVA/Ablation sample at 10 mW, where the linear red shift of the G-band switches to blue shift. The violation of linear dependence of the G-band position on the incident power is known to happen either due to mechanical deformation or doping of the SWCNTs [47,48]. As incident power increase, the water evaporation can lead to the mechanical stress of SWCNT by polymer matrix deformation. P-doping of SWCNTs by the products of PVA decomposition is also possible reason for the non-monotonic G-band shift. Any of these processes indicates on PVA matrix degradation leading to irreversible deterioration of the SA properties and decreasing its operation lifetime. In this region, we cannot recover the temperature and show its extrapolation with a dashed line. The extrapolation should be considered with caution because both optical and thermal properties of the sample might have changed under a strong illumination [21,22]. Here we also observe a deviation from the linear dependence of the laser output power on the pump power towards smaller values that indicates on the increasing nonsaturable losses of the sample (see Fig. 6). At the same time, we do not observe any significant changes in the pulse parameters. In contrast to discussed complex Raman shift behavior, aerosol SWCNTs have linear dependence of Raman shift on incident power until it is very close to the burning point. It also shows no change from cycle to cycle. The heating temperature for the Aerosol SWCNTs exceeds slightly those for PVA/HiPco at the same incident power. The reason can be understood from the Comsol modeling (see SI, section 5). The thermal conductance for the PVA composite is nearly 500 time smaller, however, the sample is 1500 times thicker. In PVA composite the heat source is distributed within 60 μm long cylinder, whereas in Aerosol SWCNTs the same optical power is applied on 40 nm film.

Our findings demonstrate that the processes governing

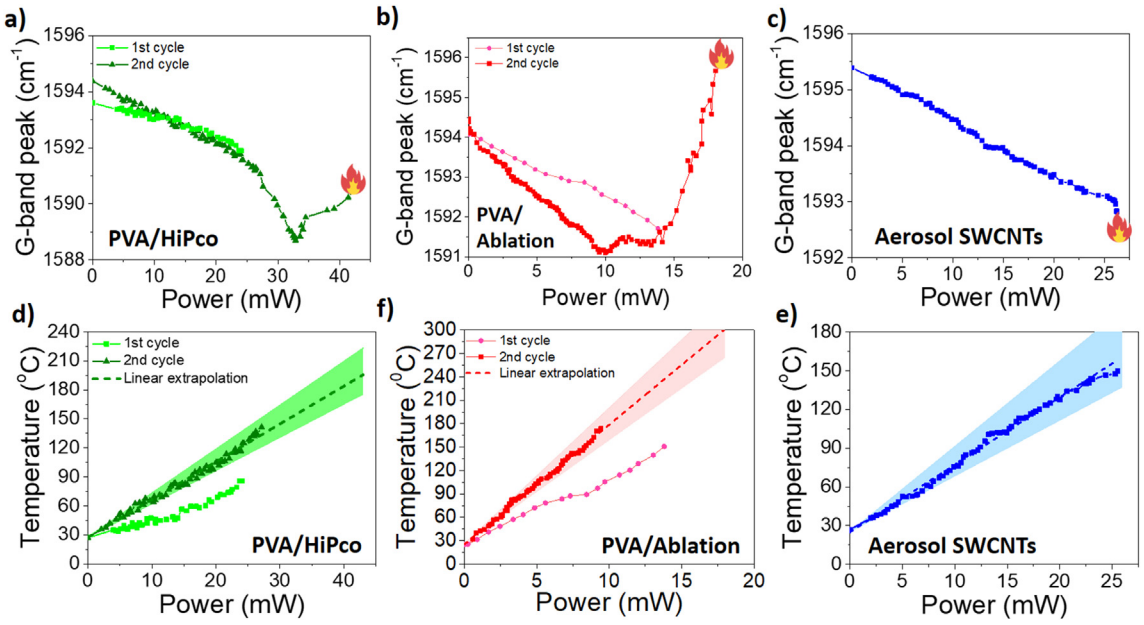

Fig. 5. The position of the G-band peak (a–c) as a function of the incident power and (d–e) corresponding temperature taken into account only linear part of the Raman shift. Dashed line is extrapolation assuming linear heating. The shaded region represents the uncertainty in temperature determination from Raman band shift coefficient. The fire icon indicates the burning point of SWCNT-SA. (A colour version of this figure can be viewed online.)

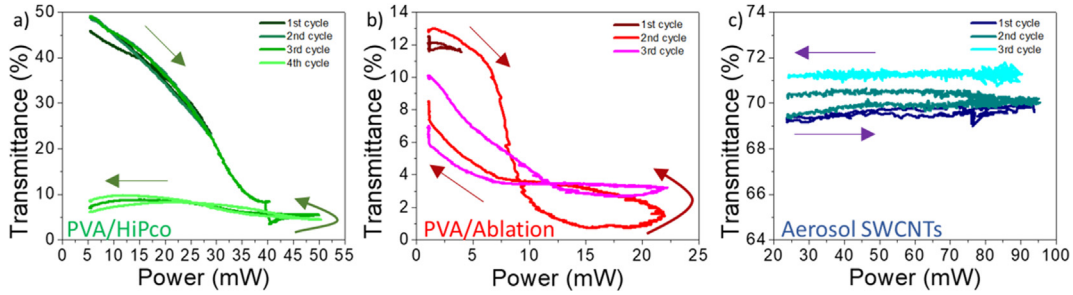

Fig. 6. The transmittance of the SWCNT-SA samples on the fiber ferrules under CW illumination as a function of the incident power, scanned from initial small signal to the higher power and back. (A colour version of this figure can be viewed online.)

degradation of the PVA composite sample and polymer-free aerosol SWCNTs have different nature. The composite samples demonstrate gradual deterioration in properties of the SWCNT-SA which happens around the temperature of the PVA decomposition. It leads to the conclusion that the damage threshold of these samples is defined by the average power of the incident light.

For Aerosol SWCNTs we observe a sample damage at the temperature around 150 °C which is well below 420 °C expected from the TGA measurements, indicating the high peak power of the ultra-short pulse to be responsible for the SWCNT-SA degradation.

To confirm this hypothesis, we measured the transmittance of the samples under continuous wave illumination. We performed the cycled measurements where we gradually increased and then decreased the incident power. The typical transmittance behavior of the samples is shown in Fig. 6. The PVA-based composites show transmittance decrease under strong illumination. In Ref. [21], this behavior is attributed to the crater formation by the intense pulse illumination and subsequent scattering by the surface roughness. We also observe sometimes formation of the crater on the composite samples. However, this mechanism alone cannot describe all observed behavior: under a small power illumination the transmittance is reversible, i.e. it returns to the initial value. For high incident power, the transmittance is not fully recovered, and the resulting transmittance depends on the illumination time. The same behavior is observed for PVA composited under pulsed illumination, where absorption saturation is followed by decrease in transmittance (Fig. S5). The average power needed for irreversible changes is nearly the same for pulsed and CW illumination. Aerosol SWCNTs can withstand much higher CW power compared to pulsed illumination (90 mW for CW and 25 mW for pulsed) and show no changes in transmittance under illumination below the threshold. To describe the higher sensitivity of polymer-free carbon nanotubes to the peak power, we propose the following mechanism. It was shown that increased defectiveness [54], amorphous carbon and catalyst nanoparticle residuals, presence of metallic carbon nanotubes [49,55] can reduce the burning threshold of the carbon nanotubes. In case of a polymer composite, a SWCNTs are coated with the matrix material that not only acts as a heat adsorbent with a certain capacity, but also protects the nanotube from a direct interaction with ambient containing oxidizing agents like oxygen, water etc. A polymer-free SWCNTs form a dense randomly oriented network of contacting nanotubes. The heat release from the exothermic reaction of the nanotube oxidation might be enough to ignite neighboring carbon nanotubes leading to

destruction of the entire network under illumination [50]. Thus, we expect the composite SWCNT-SA to be more stable for high peak power pulse generation with low repetition rate, whereas polymer-free carbon nanotubes are more suitable for high repetition rate lasers when the high peak power is not desired.

It is worth noting, the proposed method for the saturable absorber temperature measurement inside the cavity can be expanded on the other materials which has strong Raman band dependence on temperature including graphene [51], phosphorene [52] or inorganic nanostructures [53].

4. Conclusion

We have investigated the degradation mechanism of the PVA composite and polymer-free carbon nanotube saturable absorbers by measuring the heating temperature of the sample between connectors by the shift of the Raman G band. For the laser employed, the parameters of the pulse generation depend weakly on the saturable absorber properties, but the stability and even the degradation mechanism shows strong dependence on the sample preparation technique. We show that with an incident power of 20 mW the temperature on can exceed 100 °C on 30% absorbing sample. Under illumination PVA polymer composites demonstrate the gradual deterioration of the optical properties governed by thermal decomposition of the polymer matrix. In contrast, polymer-free SWCNT-SA shows no change in optical properties under illumination below the threshold defined by the peak power. Exceeding the threshold leads to the instant burning of the illuminated part of the sample. The developed technique allows to optimize the parameters of the saturable absorber and maximize the stability for required pulse regime.

Materials and methods

PVA sample preparation. 2 mg (for the HiPco composite) and 8 mg (for the Ablation composite) of SWCNTs dispersed in 10 ml of deionized with an assistance of 10 mg of sodium dodecylbenzene sulfonate (SDBS) surfactant. The aqueous solution mixture of SWCNTs was ultrasonicated for 1 h using high power ultrasonic system (Nanoruptor) operated at 250 W and 21 kHz. A well-dispersed SWCNTs obtained by the above process was subjected to ultracentrifugation (Beckman Coulter Optima Max-XP, MLS 50 rotor) for 1 h at 25000 rpm for the sedimentation of undispersed and aggregated bundles. The supernatant liquid obtained from the ultracentrifugation contains homogeneous dispersion of individualized SWCNTs. For the preparation of nanotube-polymer nanocomposite freestanding film, 1 g of polyvinyl alcohol (Wako ltd, no. 160−08295) was mixed to the homogeneously dispersed SWCNTs. The resulting suspension was poured into a Perti Dish and placed in a desiccator for one week to evaporate water. After this process, the black film formed was removed from the Perti Dish, and free-standing film was obtained. The samples were clamped between two standard (9/125 μm) fiber with index matching gel Thorlabs G608 N.

Aerosol SWCNTs preparation. Tubular quartz reactor was employed to produce SWCNTs via aerosol (floating catalyst) chemical vapor deposition method (CVD). Ferrocene (Sigma Aldrich) was used as a catalyst precursor while carbon monoxide (99.99% Linde gas) acted as a carbon source and carrier gas. In typical synthesis, ferrocene vapor (1 Pa) was injected with CO stream into the reactor. Ferrocene decomposition (~400 °C) was followed by aerosol catalyst iron particle growth and Boudouard reaction ($2CO = C + CO_2$) to nucleate a nanotube on Fe surface. Small additives concentrations of carbon dioxide tunes SWCNT diameter and, consequently, S_{11} transition position [30]. The aerosol of SWCNTs was then collected by a simple filtration on nitrocellulose filter (HAWP, Merck Millipore) to form a thin film of a desired thickness (controlled by deposition time) and could be easily dry transferred to practically any other substrate.

Sample characterization. Transmittance spectra were measured with spectrophotometer Lambda 1050 UV Vis-NIR. Raman spectra from the films were measured with Thermo Scientific DXRxi Raman Imaging Microscope with a laser wavelength of 532 nm. For temperature dependent measurements, a heating stage Linkam FTIR600 with a transparent window was employed. For all the Raman measurements, all the samples were pre-heated to nearly 150 °C to ensure reproducible measurements.

Laser scheme. The ring cavity fiber laser has a 37 cm of highly doped EDF (SM-ESF-7/125) pumped through the fiber WDM, isolator, 50/50 output coupler and fiber ferrules for integration of SWCNT-SA with a 9 μm core diameter. The pump laser diode (LD) operates at a wavelength of 1480 nm with the maximum output power of 320 mW. The full length of the laser resonator is around 5 m.

TGA and DSC with MS were conducted using NETZSCH STA 449 F3 Jupiter® unit coupled with 403 Aëolos Quadro quadrupole mass spectrometer (NETZSCH-Gerätebau GmbH, Germany). The composites were put into alumina crucibles and heated to 800 °C with a rate 5 °C/min, in dry air; flow rate 70 sccm. We employed SiC furnace in these experiments which was vacuumed prior to each measurement. The monitored mass-to-charge ratios (m/z) ranged from 10 to 110 during the heating ramp.

In-line Raman measurement setup. The Coherent Verdi laser emitting at 532 nm is free-space coupled to the fiber laser through the standard WDM. Prior to WDM, 5% of fiber laser power is out-coupled with standard fiber splitter to monitor the fiber laser power with Thorlabs S122C sensor. The signal is collected through the fiber laser output, where the green laser and fiber laser signals are filtered out by free space edge filters. The Raman signal is coupled to the Princeton Instruments Acton SP2750 spectrometer, where diffraction grating with 1800 grooves/mm is used.

Transmittance measurement. The transmittance of the SWCNT-SA samples was measured with self-build CW fiber laser and amplifier. The measurement is performed with CLD1015 laser driver and power meter consoles with S132C sensors.

CRediT authorship contribution statement

Diana Galiakhmetova: Investigation, Writing – original draft. **Yuriy Gladush:** Conceptualization, Methodology, Writing – review & editing, Software, Supervision, Writing – original draft. **Aram Mkrtchyan:** Investigation. **Fedor S. Fedorov:** Investigation, Writing – original draft. **Eldar M. Khabushev:** Investigation. **Dmitry V. Krasnikov:** Investigation, Writing – review & editing. **Raghavan Chinnambedu-Murugesan:** Investigation. **Egor Manuylovich:** Investigation. **Vladislav Dvoyrin:** Investigation, Supervision. **Alex Rozhin:** Investigation, Supervision, Writing – review & editing. **Mark Rümmeli:** Investigation, Supervision. **Sergey Alyatkin:** Investigation. **Pavlos Lagoudakis:** Conceptualization, Supervision, Writing – review & editing. **Albert G. Nasibulin:** Conceptualization, Supervision, Writing – review & editing.

Declaration of competing interest

The authors declare that they have no known competing financial interests or personal relationships that could have appeared to influence the work reported in this paper.

Acknowledgements

A.A.M. and A.G.N. thanks RFBR research project № 20-32-90233 for support in experimental part of the work. D.V.K. thanks Russian Science Foundation grant No. 20-73-10256 for support in synthesis of aerosol SWCNT films. V.D. thanks the Russian Science Foundation (Grant No. 17-72-30006) for the support in characterization of pulse laser generation.

Appendix A. Supplementary data

Supplementary data to this article can be found online at https://doi.org/10.1016/j.carbon.2021.08.032.

References

[1] S. Yamashita, Nonlinear optics in carbon nanotube, graphene, and related 2D materials, APL Photonics 4 (2019), 034301, https://doi.org/10.1063/1.5051796.
[2] S.Y. Set, H. Yaguchi, Y. Tanaka, M. Jablonski, Y. Sakakibara, A. Rozhin, M. Tokumoto, H. Kataura, Y. Achiba, K. Kikuchi, Mode-locked fiber lasers based on a saturable absorber incorporating carbon nanotubes, in: Opt. Fiber Commun. Conf., Optical Society of America, 2003, p. PD44. http://www.osapublishing.org/abstract.cfm?URI=OFC-2003-PD44.
[3] M. Chernysheva, A. Rozhin, Y. Fedotov, C. Mou, R. Arif, S.M. Kobtsev, E.M. Dianov, S.K. Turitsyn, Carbon nanotubes for ultrafast fibre lasers, Nanophotonics 6 (2017), https://doi.org/10.1515/nanoph-2015-0156.
[4] L. Huang, Y. Zhang, X. Liu, Dynamics of carbon nanotube-based mode-locking fiber lasers, Nanophotonics 9 (2020), https://doi.org/10.1515/nanoph-2020-0269.
[5] Z. Yu, Y. Wang, X. Zhang, X. Dong, J. Tian, Y. Song, A 66 fs highly stable single wall carbon nanotube mode locked fiber laser, Laser Phys. 24 (2014) 15105, https://doi.org/10.1088/1054-660X/24/1/015105.
[6] D. Popa, Z. Sun, F. Torrisi, T. Hasan, F. Wang, A. Ferrari, Generation of 63-nJ pulses from a fiber oscillator mode-locked by nanotubes, Opt. InfoBase Conf. Pap. (2010) 1–2, https://doi.org/10.1364/CLEO.2010.JTuD50.
[7] S. Kivistö, T. Hakulinen, A. Kaskela, B. Aitchison, D.P. Brown, A.G. Nasibulin, E.I. Kauppinen, A. Härkönen, O.G. Okhotnikov, Carbon nanotube films for ultrafast broadband technology, Opt Express 17 (2009) 2358, https://doi.org/10.1364/OE.17.002358.
[8] A.G. Rozhin, Y. Sakakibara, S. Namiki, M. Tokumoto, H. Kataura, Y. Achiba, Sub-200-fs pulsed erbium-doped fiber laser using a carbon nanotube-polyvinylalcohol mode locker, Appl. Phys. Lett. (2006), https://doi.org/10.1063/1.2172398.
[9] A. V Tausenev, E.D. Obraztsova, A.S. Lobach, A.I. Chernov, V.I. Konov, P.G. Kryukov, A. V Konyashchenko, E.M. Dianov, 177fs erbium-doped fiber laser mode locked with a cellulose polymer film containing single-wall carbon nanotubes, Appl. Phys. Lett. 92 (2008) 171113, https://doi.org/10.1063/1.2918450.
[10] T. Hasan, Z. Sun, F. Wang, F. Bonaccorso, P.H. Tan, A.G. Rozhin, A.C. Ferrari, Nanotube–polymer composites for ultrafast photonics, Adv. Mater. 21 (2009) 3874–3899, https://doi.org/10.1002/adma.200901122.
[11] A. Martinez, S. Yamashita, Multi-gigahertz repetition rate passively modelocked fiber lasers using carbon nanotubes, Opt Express 19 (2011) 6155, https://doi.org/10.1364/OE.19.006155.
[12] K. Kashiwagi, S. Yamashita, S.Y. Set, In-situ monitoring of optical deposition of carbon nanotubes onto fiber end, Opt Express 17 (2009) 5711–5715, https://doi.org/10.1364/OE.17.005711.
[13] S. Kobtsev, A. Ivanenko, Y. Gladush, B.N. Nyushkov, A. Kokhanovskiy, A. Anisimov, A. Nasibulin, Ultrafast all-fibre laser mode-locked by polymer-free carbon nanotube film, Opt Express 24 (2016) 28768, https://doi.org/10.1364/OE.24.028768.
[14] E.G. Gamaly, A. V Rode, Physics of ultra-short laser interaction with matter: from phonon excitation to ultimate transformations, Prog. Quant. Electron. 37 (2013) 215–323, https://doi.org/10.1016/j.pquantelec.2013.05.001.
[15] H.O. Jeschke, M.E. Garcia, K.H. Bennemann, Theory for the ultrafast ablation of graphite films, Phys. Rev. Lett. 87 (2001) 15003, https://doi.org/10.1103/PhysRevLett.87.015003.
[16] J. Chae, X. Ho, J.A. Rogers, K. Jain, Patterning of single walled carbon nanotubes using a low-fluence excimer laser photoablation process, Appl. Phys. Lett. 92 (2008) 173115, https://doi.org/10.1063/1.2919093.
[17] J. Chae, H. Jin, K. Jain, Large-area, high-speed patterning of carbon nanotubes using material-assisted excimer laser photoablation, Mater. Lett. 63 (2009) 1823–1825, https://doi.org/10.1016/j.matlet.2009.05.057.
[18] P.A. Danilov, A.A. Ionin, S.I. Kudryashov, S. V Makarov, N.N. Mel'nik, A.A. Rudenko, V.I. Yurovskikh, D. V Zayarny, V.N. Lednev, E.D. Obraztsova, S.M. Pershin, A.F. Bunkin, Femtosecond laser ablation of single-wall carbon nanotube-based material, Laser Phys. Lett. 11 (2014) 106101, https://doi.org/10.1088/1612-2011/11/10/106101.
[19] C. Li, D. Wang, T. Liang, X. Wang, J. Wu, X. Hu, J. Liang, Oxidation of multiwalled carbon nanotubes by air: benefits for electric double layer capacitors, Powder Technol. 142 (2004) 175–179, https://doi.org/10.1016/j.powtec.2004.04.037.
[20] S.P. Su, Y.H. Xu, C.A. Wilkie, Thermal degradation of polymer-carbon nanotube composites, Polym. Nanotub. Compos. Prep. Prop. Appl. (2011) 482–510, https://doi.org/10.1533/9780857091390.2.482.
[21] M. Chernysheva, M. Al Araimi, G.A. Rance, N.J. Weston, B. Shi, S. Saied, J.L. Sullivan, N. Marsh, A. Rozhin, Revealing the nature of morphological changes in carbon nanotube-polymer saturable absorber under high-power laser irradiation, Sci. Rep. 8 (2018) 1–9, https://doi.org/10.1038/s41598-018-24734-z.
[22] S.Y. Ryu, K.-S. Kim, J. Kim, S. Kim, Degradation of optical properties of a film-type single-wall carbon nanotubes saturable absorber (SWNT-SA) with an Er-doped all-fiber laser, Opt Express 20 (2012) 12966–12974, https://doi.org/10.1364/OE.20.012966.
[23] A. Martinez, K. Fuse, S. Yamashita, S.Y. Set, H. Yaguchi, Y. Tanaka, M. Jablonski, S. Goh, D. Wang, S. Yamashita, J. Lim, K. Knabe, K.A. Tillman, W. Neely, Y. Wang, R. Amezcua-Correa, F. Couny, P.S. Light, F. Benabid, J.C. Knight, K.L. Corwin, J.W. Nicholson, B.R. Washburn, Enhanced stability of nitrogen-sealed carbon nanotube saturable absorbers under highintensity irradiation, Opt Express 21 (2013) 4665–4670, https://doi.org/10.1364/OE.21.004665.
[24] Y.-W. Song, S. Yamashita, C.S. Goh, S.Y. Set, Carbon nanotube mode lockers with enhanced nonlinearity via evanescent field interaction in D-shaped fibers, Opt. Lett. 32 (2007) 148, https://doi.org/10.1364/OL.32.000148.
[25] Y.W. Song, S. Yamashita, S. Maruyama, Single-walled carbon nanotubes for high-energy optical pulse formation, Appl. Phys. Lett. 92 (2008) 1–4, https://doi.org/10.1063/1.2834898.
[26] A.A. Mkrtchyan, Y.G. Gladush, D.I. Galiakhmetova, V.Y. Yakovlev, V.T. Ahtyamov, A.G. Nasibulin, Dry-transfer technique for polymer-free single-walled carbon nanotube saturable absorber on a side polished fiber, Opt. Mater. Express 9 (2019), https://doi.org/10.1364/OME.9.001551.
[27] K. Kieu, M. Mansuripur, Femtosecond laser pulse generation with a fiber taper embedded in carbon nanotube/polymer composite, Opt. Lett. 32 (2007) 2242–2244, https://doi.org/10.1364/OL.32.002242.
[28] A. Martinez, M. Al Araimi, A. Dmitriev, P. Lutsyk, S. Li, C. Mou, A. Rozhin, M. Sumetsky, S. Turitsyn, Low-loss saturable absorbers based on tapered fibers embedded in carbon nanotube/polymer composites, APL Photonics 2 (2017) 126103, https://doi.org/10.1063/1.4996918.
[29] C. Mou, A. Rozhin, R. Arif, K. Zhou, S. Turitsyn, Polarization insensitive in-fiber mode-locker based on carbon nanotube with N-methyl-2-pyrrolidone solvent filled fiber microchamber, Appl. Phys. Lett. 100 (2012) 101110, https://doi.org/10.1063/1.3691922.
[30] P. V Huong, R. Cavagnat, P.M. Ajayan, O. Stephan, Temperature-dependent vibrational spectra of carbon nanotubes, Phys. Rev. B 51 (1995) 10048–10051, https://doi.org/10.1103/PhysRevB.51.10048.
[31] M. He, E. Rikkinen, Z. Zhu, Y. Tian, A. Anisimov, H. Jiang, A. Nasibulin, E. Kauppinen, M. Niemelä, A. Krause, Temperature dependent Raman spectra of carbon nanobuds, J. Phys. Chem. C 114 (2010), https://doi.org/10.1021/jp104004a.
[32] M.H. Rümmeli, C. Kramberger, M. Löffler, O. Jost, M. Bystrzejewski, A. Grüneis, T. Gemming, W. Pompe, B. Büchner, T. Pichler, Catalyst volume to surface area constraints for nucleating carbon nanotubes, J. Phys. Chem. B 111 (2007) 8234–8241, https://doi.org/10.1021/jp072556f.
[33] E.M. Khabushev, D. V Krasnikov, O.T. Zaremba, A.P. Tsapenko, A.E. Goldt, A.G. Nasibulin, Machine learning for tailoring optoelectronic properties of single-walled carbon nanotube films, J. Phys. Chem. Lett. 10 (2019) 6962–6966, https://doi.org/10.1021/acs.jpclett.9b02777.
[34] A. Kaskela, A.G. Nasibulin, M.Y. Timmermans, B. Aitchison, A. Papadimitratos, Y. Tian, Z. Zhu, H. Jiang, D.P. Brown, A. Zakhidov, E.I. Kauppinen, Aerosol-synthesized SWCNT networks with tunable conductivity and transparency by a dry transfer technique, Nano Lett. 10 (2010) 4349–4355, https://doi.org/10.1021/nl101680s.
[35] K. Ramadurai, C. Cromer, A. Dillon, R. Mahajan, J. Lehman, Raman and electron microscopy analysis of carbon nanotubes exposed to high power laser irradiance, J. Appl. Phys. 105 (2009) 93106, https://doi.org/10.1063/1.3116165.
[36] B.G. Bale, O.G. Okhotnikov, S.K. Turitsyn, Modeling and technologies of ultrafast fiber lasers, in: G.O. Oleg (Ed.), Fiber Lasers, Wiley-VCH Verlag, Germany, 2012, pp. 135–176, https://doi.org/10.1002/9783527648641.ch5.
[37] E.J. Lee, S.Y. Choi, H. Jeong, N.H. Park, W. Yim, M.H. Kim, J.-K. Park, S. Son, S. Bae, S.J. Kim, K. Lee, Y.H. Ahn, K.J. Ahn, B.H. Hong, J.-Y. Park, F. Rotermund, D.-I. Yeom, Active control of all-fibre graphene devices with electrical gating, Nat. Commun. 6 (2015) 6851, https://doi.org/10.1038/ncomms7851.
[38] Y. Gladush, A.A. Mkrtchyan, D.S. Kopylova, A. Ivanenko, B. Nyushkov, S. Kobtsev, A. Kokhanovskiy, A. Khegai, M. Melkumov, M. Burdanova, M. Staniforth, J. Lloyd-Hughes, A.G. Nasibulin, Ionic liquid gated carbon nanotube saturable absorber for switchable pulse generation, Nano Lett. 19 (2019) 5836–5843, https://doi.org/10.1021/acs.nanolett.9b01012.
[39] Y. Tsuchiya, K. Sumi, Thermal decomposition products of poly(vinyl alcohol), J. Polym. Sci. Polym. Chem. 7 (1969) 3151–3158, https://doi.org/10.1002/pol.1969.150071111.
[40] A.Y. Shaulov, S.M. Lomakin, T.S. Zarkhina, A.D. Rakhimkulov, N.G. Shilkina, Y.B. Muravlev, A.A. Berlin, Carbonization of poly(vinyl alcohol) in blends with boron polyoxide, Dokl. Phys. Chem. 403 (2005) 154–158, https://doi.org/10.1007/s10634-005-0048-x.
[41] B.J. Holland, J. Hay, The thermal degradation of poly(vinyl alcohol), Polymer

42 (2001) 6775–6783, https://doi.org/10.1016/S0032-3861(01)00166-5.
[42] H. Yang, S. Xu, L. Jiang, Y. Dan, Thermal decomposition behavior of poly (vinyl alcohol) with different hydroxyl content, J. Macromol. Sci. Part B. 51 (2012) 464–480, https://doi.org/10.1080/00222348.2011.597687.
[43] P. Budrugeac, Kinetics of the complex process of thermo-oxidative degradation of poly(vinyl alcohol), J. Therm. Anal. Calorim. 92 (2008) 291–296, https://doi.org/10.1007/s10973-007-8770-8.
[44] V. Iakovlev, Y.A. Sklyueva, F.S. Fedorov, D. Rupasov, V.A. Kondrashov, A. Grebenko, K. Mikheev, F.Z. Gilmutdinov, A. Anisimov, G. Mikheev, A. Nasibulin, Improvement of optoelectronic properties of single-walled carbon nanotube films by laser treatment, Diam. Relat. Mater. 88 (2018), https://doi.org/10.1016/j.diamond.2018.07.006.
[45] Y.S. Park, Y.C. Choi, K.S. Kim, D.-C. Chung, D.J. Bae, K.H. An, S.C. Lim, X.Y. Zhu, Y.H. Lee, High yield purification of multiwalled carbon nanotubes by selective oxidation during thermal annealing, Carbon N. Y. 39 (2001) 655–661, https://doi.org/10.1016/S0008-6223(00)00152-4.
[46] Z. Shi, Y. Lian, F.H. Liao, X. Zhou, Z. Gu, Y. Zhang, S. Iijima, H. Li, K.T. Yue, S.-L. Zhang, Large scale synthesis of single-wall carbon nanotubes by arc-discharge method, J. Phys. Chem. Solid. 61 (2000) 1031–1036, https://doi.org/10.1016/S0022-3697(99)00358-3.
[47] A.M. Rao, P.C. Eklund, S. Bandow, A. Thess, R.E. Smalley, Evidence for charge transfer in doped carbon nanotube bundles from Raman scattering, Nature 388 (1997) 257–259, https://doi.org/10.1038/40827.
[48] X. Duan, H. Son, B. Gao, J. Zhang, T. Wu, G.G. Samsonidze, M.S. Dresselhaus, Z. Liu, J. Kong, Resonant Raman spectroscopy of individual strained single-wall carbon nanotubes, Nano Lett. 7 (2007) 2116–2121, https://doi.org/10.1021/nl0711155.
[49] A.E. Islam, J.A. Rogers, M.A. Alam, Recent progress in obtaining semiconducting single-walled carbon nanotubes for transistor applications, Adv. Mater. 27 (2015) 7908–7937, https://doi.org/10.1002/adma.201502918.
[50] M.P. Gupta, A. Behnam, F. Lian, D. Estrada, E. Pop, S. Kumar, High field breakdown characteristics of carbon nanotube thin film transistors, Nanotechnology 24 (2013) 405204, https://doi.org/10.1088/0957-4484/24/40/405204.
[51] I. Calizo, A.A. Balandin, W. Bao, F. Miao, C.N. Lau, Temperature dependence of the Raman spectra of graphene and graphene multilayers, Nano Lett. 7 (9) (2007) 2645–2649, https://doi.org/10.1021/nl071033g.
[52] S. Zhang, J. Yang, R. Xu, F. Wang, W. Li, M. Ghufran, Yong-Wei Zhang, Z. Yu, G. Zhang, Q. Qin, Y. Lu, Extraordinary photoluminescence and strong temperature/angle-dependent Raman responses in few-layer phosphorene, ACS Nano 8 (9) (2014) 9590–9596, https://doi.org/10.1021/nn503893j.
[53] R.D. Rodriguez, E. Sheremet, D.J. Thurmer, D. Lehmann, O.D. Gordan, F. Seidel, A. Milekhin, O.G. Schmidt, M. Hietschold, D.R.T. Zahn, Temperature-dependent Raman investigation of rolled up InGaAs/GaAs microtubes, Nanoscale Research Letters 7 (2012) 594, https://doi.org/10.1186/1556-276X-7-594.
[54] D. Bom, R. Andrews, D. Jacques, J. Anthony, B. Chen, M.S. Meier, J.P. Selegue, Thermogravimetric analysis of the oxidation of multiwalled carbon Nanotubes: evidence for the role of defect sites in carbon nanotube chemistry, Nano Lett. 2 (6) (2002) 615–619, https://doi.org/10.1021/nl020297u.
[55] D. Janas, Towards monochiral carbon nanotubes: a review of progress in the sorting of single-walled carbon nanotubes, Mater. Chem. Front. 2 (2018) 36–63, https://doi.org/10.1039/C7QM00427C.